Effects of density-dependent lepton fraction on the properties of protoneutron stars

A. Sulaksono[1] and L. Satiawati[2]
[1]*Departmen Fisika, FMIPA, Universitas Indonesia, Depok 16424, Indonesia*
[2]*Program studi Fisika, FTS, Universitas Nasional, Jakarta 12520, Indonesia*
(Received 24 February 2013; published 10 June 2013)

The density-dependent lepton fractions approach that is used to describe the properties of matter with neutrino trapping is systematically studied. It is found that two sets of the ratio of trapped neutrinos to leptons parameters—i.e., one for a relativistic mean field parameter set with stiff equation of state and one for a parameter set with soft equation of state—yield particle composition profiles at high densities similar to those predicted by the standard fixed lepton fraction approach. However, these sets of parameters produce significantly different behavior at low densities compared to those of standard approach. The consequences of applying the density-dependent lepton fractions approach to some properties of PNS, such as the particle composition, equation of state, the onset of low-density instability, the mass-radius relation, and the mean free path of electron neutrino, are investigated. By comparing the results with those of the standard approach, we obtain the result that the PNS equation of state is not significantly influenced by the low-density behavior difference between the two approaches. However, the density-dependent lepton fractions approach yields a smaller onset of low-density instability matter and core-crust transition density but a slightly larger maximum mass as well as a larger radius of canonical mass than those predicted by the standard approach. The estimated minimum PNS mass and its radius are apparently also sensitive to the parameter used for the ratio of trapped neutrinos to leptons. For electron neutrino transport in PNSs, matter with density-dependent lepton fractions is more transparent than matter with fixed lepton fractions.

DOI: 10.1103/PhysRevC.87.065802 PACS number(s): 26.60.−c, 25.30.Pt, 13.15.+g

I. INTRODUCTION

It is generally believed that a hot and dense protoneutron star (PNS) is formed just after the core collapse of a massive star in a type-II supernova explosion. The iron core of such a star collapses when its mass reaches the Chandrasekhar limit [1],

$$M_{\rm Ch} \sim 5.8 Y_e^2 \left(1 + \left(\frac{s_e}{\pi Y_e}\right)^2\right) M_\odot \sim 1.2\text{–}1.5 M_\odot, \quad (1)$$

where Y_e denotes the electron number per baryon which depends on the mass of the progenitor star, and s_e is the electron entropy per baryon (in units of Boltzmann's constant). In precollapse iron cores, typical values of Y_e are around 0.42 at the center and 0.48 at the outer edge [2]. For example, by putting $Y_e = 0.45$ and $s_e = 0.52$ of a progenitor star with $M = 15 M_\odot$ into Eq. (1), then $M_{\rm Ch} = 1.34 M_\odot$ is obtained [3]. The formed PNS is a lepton-rich star, with a matter density of $\rho = 2\text{–}6 \times 10^{14}$ g/cm^2 and a temperature of $T = 5\text{–}40$ MeV, where, in this condition, neutrinos are temporarily trapped in the PNS core and the electron-lepton fraction is essentially fixed [1,4]. The following PNS evolution is dominated by neutrino diffusion. In this stage, the star is first heated, deleptonized, and subsequently cooled. Then, it becomes a neutron star (NS) at practically zero temperature without trapped neutrinos [4–6]. We note that the microphysics input for stellar core collapse simulation come essentially from the neutrino-matter interaction rates and deleptonization, i.e., electron capture and the equation of state (EOS) [7]. To construct the EOS is indeed not easy because quite wide ranges of density (10^4–10^5 g/cm^3), temperature (0–100 MeV), and composition with proton fraction (0–0.6) should be taken into consideration. Within these ranges, the characteristics of nuclear matter change dramatically, from an ideal gas of different nuclei up to uniform strongly interacting matter. Even a transition to deconfined quark matter should be included. Presently, two hadronic EOS exist which are commonly used in core collapse simulations, i.e., by Lattimer and Swesty [8] and by Shen *et al.* [9]. These two EOS use different kinds of nuclear interactions but both take into account noninteracting α particles, a single heavy nucleus, and free nucleons, in addition to the electron, positron, and photon gas. At low densities, the composition of matter becomes much more complicated due to the large number of different nuclei involved [10], while at high densities recently a quark-hadron phase transition was indicated [11]. The effects of exotic particles such as hyperons, kaons, etc., have been discussed by many authors, e.g., Refs. [7,12]. It is worth noting that PNS cooling and convection are sensitive to the symmetry energy [13]; the nuclear symmetry energy and its density dependence have attracted much attention due to their importance in nuclear physics and astrophysics (see Ref. [14] and references therein). The mass of the PNS plays a crucial role as a unique constraint to determine the minimum NS mass [15–17].

In the standard calculations of the earliest stages of PNS evolution, the balance equations for the chemical potentials, charge neutrality, baryon number conservation, and fixed lepton fractions, all at fixed temperatures or in an isentropic process, are commonly used. In these stages, the time scale of the weak interaction is much smaller than the evolutionary time scale, i.e., neutrino diffusion time or the neutrino cooling time. The gravitational collapse calculations of the electron-degenerate core of a massive star indicate that at the onset of trapping the electron-lepton fraction $Y_{Le} = Y_e + Y_{\nu_e} \approx 0.4$ [6],

where Y_e and Y_{ν_e} are the fractions of electrons and electron neutrinos, respectively. The precise value of Y_{Le} depends on the efficiency of electron capture reactions during this initial collapse stage. When electron neutrinos become trapped, the fraction of muon leptons must be conserved, so the constraint $Y_{L\mu} = Y_\mu - Y_{\bar{\nu}_\mu} \approx 0$ is usually also imposed [6]. Here, Y_μ and $Y_{\bar{\nu}_\mu}$ are the fractions of muons and muon antineutrinos. Note that $t \sim 50$–100 ms after core bounce stage is characterized by a hot shocked envelope with an entropy per baryon of $s \sim 4$–5 for densities $\rho < 0.02$ fm^3, an unshocked core with $s \sim 1$ for densities $\rho > 0.1$ fm^3, and a transition region between these densities. At $t \sim 0.5$–1 s after core bounce stage, except in some outer regions, the entropy per baryon is approximately constant throughout the star ($s \sim 2$). This stage is modeled with a neutrino transparent envelope with densities $\rho < \rho_{\rm env} = 6 \times 10^{-4}$ fm^3 and a neutrino opaque core with densities $\rho > \rho_{\rm core}$, and the transition region between $\rho_{\rm env}$ and $\rho_{\rm core}$ is called the neutrino sphere (see Ref. [18] and references therein).

The fixed Y_{Le} and $Y_{L\mu}$ are a very good approximation for the high-density part of the core of the above PNS stages. However, in the region close to the surface, the probability of the neutrinos being trapped might depend sensitively on density and temperature. This is due to the fact that, in this region, the neutrino mean free path changes rather significantly due to the change of density and temperature and since the ratio of neutrinos to leptons determined from β equilibrium depends also on the density and temperature. Thus, it is quite reasonable to assume that the electron lepton fraction is decreasing in the region near the surface of the PNS [19]. Furthermore, at the envelope (crust) region the matter loses neutrinos very fast during the PNS evolution and, as a consequence, the trapping condition $Y_{Le} = 0.4$ does not apply any more in this region [17]. Therefore, the view of smoothly decreasing electron neutrinos near the edge physically looks more natural than the one with an abrupt change in the transition region.

To properly describe the transition from the low-density core to the envelope in PNS matter with standard fixed Y_{Le}, the neutrino sphere concept should be introduced. From recent studies, however, it is known that the location of the neutrino sphere is uncertain [15–17,20]. Typical model-dependent values for the location of the neutrino sphere found in the literature are 2×10^3 fm^3 [15], 6×10^4 fm^3 [18], and 2×10^5 fm^3 [20]. The authors of Ref. [17] choose the cutoff procedure; i.e., by imposing the condition $Y_{Le} = 0.4$ at any density in a certain threshold density range $\rho_\nu \approx 10^5$–10^6 fm^3 until the electron fraction Y_e becomes 0.4, the neutrinos disappear naturally. This means that the minimum mass of the (P)NS predicted by using the standard fixed Y_{Le} approach for the core is also sensitive to the model of neutrino sphere used. If the Y_{Le} in the low-density part of the core is density dependent and significantly smaller than 0.4, the natural smooth transition from the core to the envelope can be more easily reached and its impact might shed light on the neutrino sphere uncertainty problem.

Recently, Ryu *et al.* [19] studied the EOS of the core of the early stage of a PNS by using the relativistic mean field (RMF) model with the density-dependent fractions of lepton (DDYL) approach for the isentropic process and the entropy density $s = 2$. The EOS is obtained by assuming that the ratio of trapped neutrinos to leptons as a function of baryon density fulfills the following relations: $\rho_{\nu_e} \equiv x_e(\rho_B)\rho_e$ and $\rho_{\nu_\mu} \equiv x_m(\rho_B)\rho_\mu$, where $x_i(\rho_B)$ reads [19]

$$x_i(\rho_B) = x_{0i}\{1 - \exp[-\beta(\rho_B/\rho_0)^\gamma]\}, \quad i = e, m. \qquad (2)$$

The specific values $x_{0e} = x_{0m} = x_0 \equiv 0.3$, $\beta \equiv 0.05$, and $\gamma \equiv 2$ were used in that work in order that the ratio $x_i(\rho_B) = x(\rho_B)$ produce a smooth smearing of leptons at the surface of a PNS while maintaining $x < 0.5$ in all regions of the PNS [19]. They stated that the profile of neutrino population at high density which is found is consistent with those calculated by using the neutrino transport theory [21,22], and they also used this approach to study the change of the spin period due to the neutrino emission from the PNS [23]. However, there is one thing that attracts our attention from their results. The parameter value $x_0 \equiv 0.3$ in Ref. [19] obtained due to their EOS is very soft, but the predicted Y_{Le} is about 0.4 at high densities; or their EOS is moderately soft but Y_{Le} is less than 0.4 at high densities. By using a set of well known RMF parameter sets from the literature and the $T = 0$ approximation, it is found that x_0 is quite sensitive to the parameter set used; in order to maintain $Y_{Le} \sim 0.4$ at high densities, x_0 should be $\leqslant 0.3$ for all RMF parameter sets used.

In the present work, we explore the acceptable value of each parameter in Eq. (2) by taking a different way than the one used in Ref. [19]. The equality between x_{0e} and x_{0m} is relaxed to provide more flexibility of the $x_i(\rho_B)$. For determining x_{0e} and x_{0m}, physical constraints are used, i.e., $Y_{Le} \approx 0.4$ at high densities and $Y_{L\mu} \approx 0$ at all densities. These constraints are more restricted the one used in Ref. [19] so that the constraint in Ref. [19] is automatically fulfilled and the right density for the appearance of the first muon is properly predicted. The β and γ parameters are adjusted to get a result closer to the one predicted by using the conventional constant lepton fractions (CYL) approach [6,18]. In this way, we can get predictions of the fraction of every constituent at high densities similar to the ones obtained by the standard CYL approach but with significantly different behavior at low densities. Note that in this work we used $\rho_{\bar{\nu}_\mu} \equiv x_m(\rho_B)\rho_\mu$ instead of $\rho_{\nu_\mu} \equiv x_m(\rho_B)\rho_\mu$. We also investigate the behavior of $x_i(\rho_B)$ with respect to the variation of x_{0m}, β, and γ parameters to check the limitation of the parametrization. Because x_{0e} is quite sensitive to the parameter set used, two RMF parameter sets are employed, i.e., NL3 [24] which represents a stiff EOS, and IUFSU* [25] which represents relatively soft EOS. To demonstrate the sensitivity of the $x_i(\rho_B)$ parameters with respect to the parameter set variation, the fractions of leptons predicted by BSP [25], G1 and G2 [26], GM1 [27], and FSU [28] parameter sets are also calculated. To see the explicit effects of implementing the DDYL approach in PNS observables, the low-density instability of PNS matter, the PNS mass-radius relation, and the electron-neutrino mean free path are calculated and the results are compared to the ones obtained by using CYL.

Note that, unlike the case of NS matter (matter without neutrino trapping) where some efforts have been devoted (Ref. [29] and references therein), the core-crust transition density ρ_t and the onset of the instability region for matter with neutrino trapping are rarely explored. For the case of

matter with neutrino trapping using the CYL approach, it is known that ρ_t and the onset of the unstable region are relatively larger than the ones for matter without neutrino trapping [30–32]. A quite strong Coulomb interaction produced by the interaction among protons and electrons at low density, which is larger than the repulsive isovector interaction created by the asymmetry in the nucleon numbers at this density, is the agent to make this happen. However, why a strong Coulomb interaction can be present in low-density matter with trapped neutrinos is not yet fully understood. We also need to note that neutrino mean free paths in a PNS are significantly altered by the effect of the strong interaction and by the multicomponent nature of dense matter [22]. The importance of correlations in neutrino transport in dense and hot matter has been also discussed by many authors (see Ref. [33] and references therein), and for a PNS with CYL it was reported in Ref. [34] that the random phase approximation (RPA) corrections with respect to the mean field approximation are only 10% to 15% at high density. However, it has been known for some time that the RPA corrections indeed could lead to significant changes in mean free path, compared to the mean field approximation (see, e.g., Refs. [35,36]). The effect of neutrino electromagnetic form factors on the neutrino cross section in a PNS with CYL has been already discussed in Ref. [37].

Since in this work we focus on the effect of DDYL on the compositional variables of PNS matter, the $T = 0$ approximation is used just to simplify the analysis. This approximation is quite reasonable because, in a P(NS), the compositional variables of the EOS play a more important role than the temperature [6], and the DDYL has significant effect only in the relatively low-density region which is also much colder than the center of the core. For the same reason, in the calculation of the electron-neutrino mean free path, the RPA correlation, finite-temperature effect, hyperons, and other exotic contributions are not considered.

Section II presents the formulation of the DDYL matter model and a discussion on the particle composition in matter with neutrino trapping. Low-density instability is discussed in Sec. III, the mass-radius relation of a PNS is discussed in Sec. IV, while the electron-neutrino mean free path in a PNS is discussed in Sec. V. Finally, conclusions are given in Sec. VI.

II. DENSITY-DEPENDENT LEPTON FRACTION AND MATTER MODEL

In this section, the effect of DDYL on the particle composition in matter with neutrino trapping is systematically studied. The β equilibrium conditions and the Lagrangian density that are used to describe the system are given and after that the calculation results are discussed.

To determine the fraction of every constituent in matter with neutrino trapping, the following constraints are used

(i) Balance equations for chemical potentials:

$$\mu_n + \mu_{\nu_e} = \mu_p + \mu_e, \quad \mu_e - \mu_{\nu_e} = \mu_\mu + \mu_{\bar{\nu}_\mu}. \tag{3}$$

(ii) Charge neutrality:

$$\rho_e + \rho_\mu = \rho_p. \tag{4}$$

(iii) Conservation of total density of baryons:

$$\rho_B = \rho_n + \rho_p. \tag{5}$$

In addition, for the conventional CYL approach, the following values are usually adopted:

$$Y_{Le} = Y_e + Y_{\nu_e} \approx 0.4, \tag{6}$$

$$Y_{L\mu} = Y_\mu - Y_{\bar{\nu}_\mu} \approx 0, \tag{7}$$

while in the case of DDYL, because $\rho_{\nu_e} = x_e(\rho_B)\rho_e$ and $\rho_{\bar{\nu}_\mu} = x_m(\rho_B)\,\rho_\mu$ are assumed, then

$$Y_{Le} = [1 + x_e(\rho_B)]\, Y_e \tag{8}$$

and

$$Y_{L\mu} = [1 - x_m(\rho_B)]\, Y_\mu. \tag{9}$$

To describe PNS matter in the mean field approximation, the following RMF Lagrangian density is employed:

$$\mathcal{L} = \mathcal{L}_N^{\rm lin} + \mathcal{L}_M^{\rm lin} + \mathcal{L}_{\rm nonlin} + \mathcal{L}_L,$$

where the first three terms are used to describe the nucleons (p, n) and the last term is the free Lagrangian for leptons (e, μ, ν_e, and $\bar{\nu}_\mu$). The first term is the standard linear Lagrangian for nucleons, where each nucleon interacts with the others via meson exchange. The second is the linear meson Lagrangian (σ, ω, and ρ) and the third is the nonlinear mesons self-interaction Lagrangian. The general nonlinear meson self-interaction Lagrangian is [25]

$$\begin{aligned}\mathcal{L}_{\rm nonlin} = &-\frac{\kappa_3}{6M} g_\sigma m_\sigma^2 \sigma^3 - \frac{\kappa_4}{24M^2} g_\sigma^2 m_\sigma^2 \sigma^4 \\ &+ \frac{1}{24}\zeta_0 g_\omega^2 (\omega_\mu \omega^\mu)^2 + \frac{\eta_{2\rho}}{4M^2} g_\omega^2 m_\rho^2 (\omega_\mu \omega^\mu)(\rho_\nu \rho^\nu) \\ &+ \frac{\eta_1}{2M} g_\sigma m_\omega^2 \sigma (\omega_\mu \omega^\mu) + \frac{\eta_2}{4M^2} g_\sigma^2 m_\omega^2 \sigma^2 (\omega_\mu \omega^\mu) \\ &+ \frac{\eta_\rho}{2M} g_\sigma m_\rho^2 \sigma (\rho_\mu \rho^\mu) + \frac{\eta_{1\rho}}{4M^2} g_\sigma^2 m_\rho^2 \sigma^2 (\rho_\mu \rho^\mu),\end{aligned} \tag{10}$$

where σ, ω, and ρ are the meson fields while g_σ, g_ω, and g_ρ are their corresponding coupling constants. m_σ, m_ω, m_ρ, and M are the σ, ω, ρ, and nucleon masses while κ_3, κ_4, ζ_0, η_1, η_2, η_ρ, $\eta_{1\rho}$, and $\eta_{2\rho}$ are the nonlinear meson self-interaction parameters, respectively.

In the present calculation, we use NL3 as a representation of the stiff EOS and IUFSU* as a representation of the soft EOS parameter sets for thorough investigations while, to observe the effect of the parameter set variation on each fraction of all leptons involved by using the DDYL approach, G1, G2, GM1, FSU, and BSP parameter sets are used. These parameter sets differ from each other due to the nonzero terms in Eq. (10).

In the following, we will discuss how to obtain the parameters of $x_i(\rho_B)$ used in this work. As was already mentioned in Introduction, the constraint $Y_{Le} \sim 0.4$ at high densities makes the predicted x_{0e} depend on the parameter set used. For NL3, $x_{0e} \sim 0.08$ is needed, but for IUFSU*,

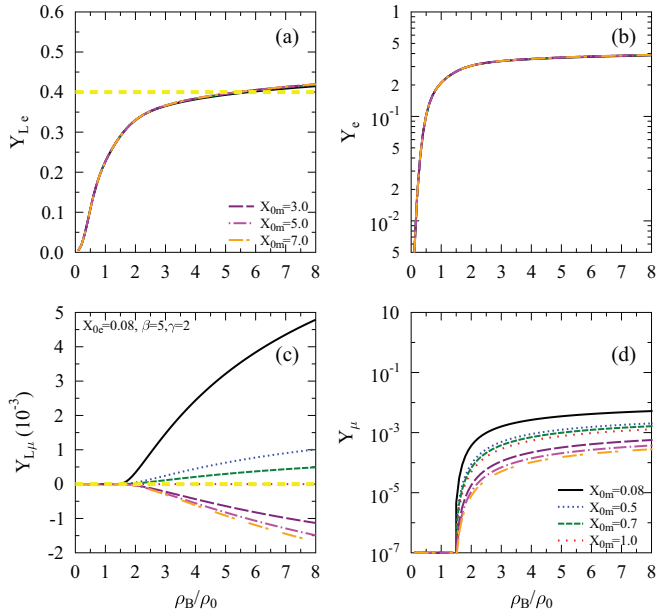

FIG. 1. (Color online) The effect of the X_{0m} variation on the fractions of leptons. The NL3 parameter set and DDYL approach are used. The fraction of (a) electron leptons, (b) electrons, (c) muon leptons, and (d) muons.

$x_{0e} \sim 0.2$ is needed to fulfill this constraint, while the values of other parameters of $x_i(\rho_B)$ indeed depend on their corresponding x_{0e} value. In the case of NL3, for instance, if we use $x_{0e} = 0.08$ and choose $\gamma = 2$ and $\beta = 5$, only a typical value $x_{0m} \sim 1.0$ can fulfill the $Y_{L\mu} \sim 0$ requirement. This x_{0m} value fixes also the average Y_μ prediction at high densities. This condition is clearly captured in Fig. 1. As is shown in Fig. 2, in the case of IUFSU*, if we use $x_{0e} = 0.2$ and choose for instance $\gamma = 0.5$ and $\beta = 1.03$, an increase in x_{0m} causes a

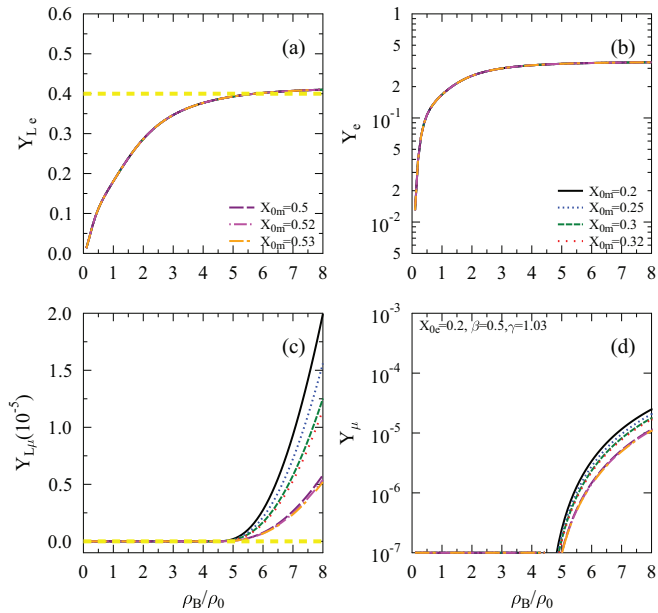

FIG. 2. (Color online) Similar to Fig. 1 but predicted by the IUFSU* parameter set.

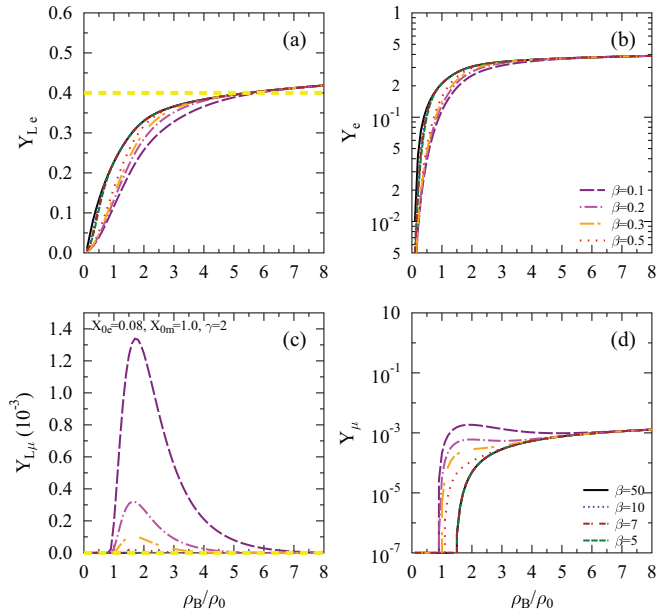

FIG. 3. (Color online) The effect of the β variation on lepton fractions predicted by the NL3 parameter set using the DDYL approach.

decrease in $Y_{L\mu}$ at high densities. However, up to $x_{0m} \sim 0.3$ the change of $Y_{L\mu}$ becomes less significant by increasing x_{0m}, and around this x_{0m} value at $\rho_B \geqslant 6\ \rho_0$ the $Y_{L\mu}$ is already about 10^{-5}. Therefore, in the IUFSU* case we can fix $x_{0m} \sim 0.3$. However, different from the NL3 case, the variation of x_{0m} in the case of IUFSU* does not significantly influence Y_μ. In Figs. 3 and 4, the β and γ variations in $x_i(\rho_B)$ for the NL3 case are presented by using $x_{0e} \sim 0.08$ and $x_{0m} \sim 1.0$ while in Figs. 5 and 6 are those for the case IUFSU* by using $x_{0e} \sim 0.2$

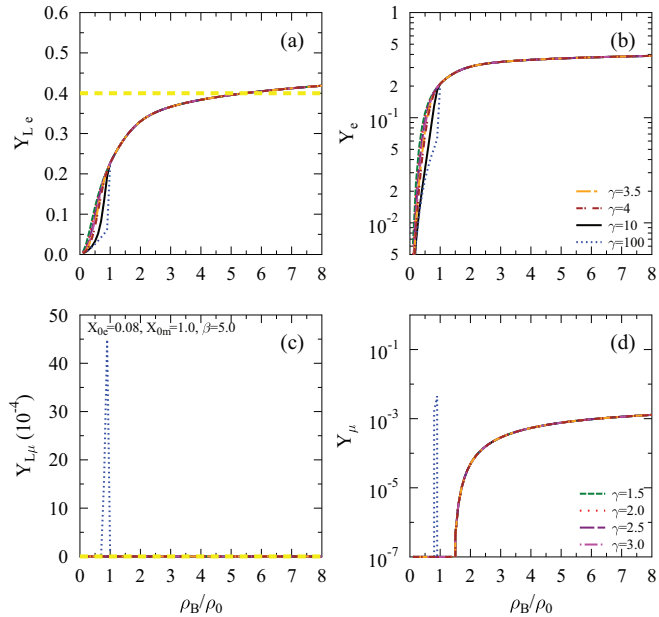

FIG. 4. (Color online) The effect of the γ variation on lepton fractions predicted by the NL3 parameter set using the DDYL approach.

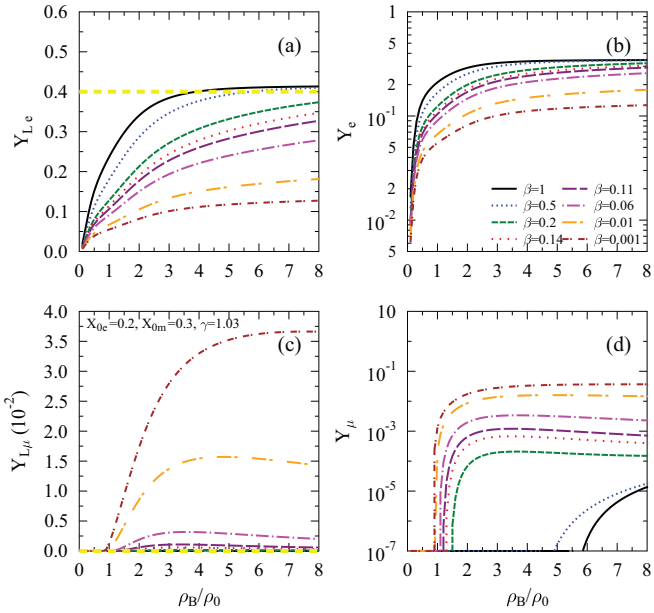

FIG. 5. (Color online) Similar to Fig. 3 but predicted by the IUFSU* parameter set.

and $x_{0m} \sim 0.3$. For the NL3 case, it is obvious, if $\beta = 5$ is taken, that $Y_{L\mu}$ and Y_μ are almost unaffected by a relatively large range of γ variation (up to $\gamma < 100$). For $\gamma \geqslant 100$, an unnaturally sharp peak of the "appearing and disappearing" muons presents even at $\rho_B < \rho_0$. However, the low-density behaviors of Y_{Le} and Y_e are quite sensitive with respect to γ variation, and the effect becomes significant for $\gamma \geqslant 4$. On the other hand, if we take $\gamma = 2$, the fractions of all leptons are quite sensitive to β variation. The requirement $Y_{L\mu} \sim 0$ is reached if $\beta \geqslant 0.5$ is taken. No significant change in Y_μ has

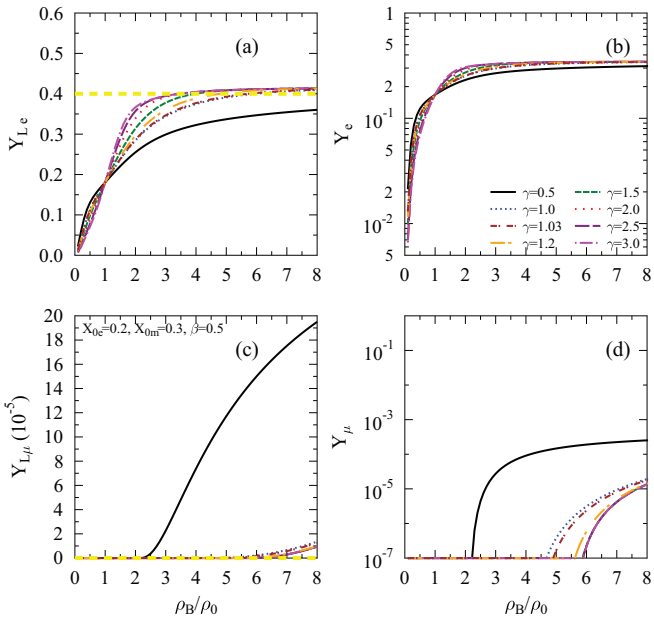

FIG. 6. (Color online) Similar to Fig. 4 but predicted by the IUFSU* parameter set.

been observed by varying $\beta \geqslant 10$. Therefore, for the NL3 case, $\beta = 5$ and $\gamma = 2$ is a quite appropriate choice. This choice already takes into consideration that the prediction of the first muon appearance is closer to the one predicted by the CYL approximation. In the case of IUFSU* on the other hand, the fractions of all leptons are quite sensitive to β and γ variations. If for instance $\gamma = 1.03$ is chosen, it can be observed that Y_{Le} is quite sensitive to β variation. Only by using $\beta \geqslant 0.5$ can the requirement $Y_{Le} \sim 0.4$ at high densities be ensured. In this typical range, $Y_{L\mu}$ is not significantly affected by β variation, even though the starting density of the appearance of the first muon rather depends on this parameter. On the other hand, if we take $\beta = 0.5$ then $Y_{L\mu}$ becomes quite sensitive to γ variation, and, starting form $\gamma = 1$, $Y_{L\mu}$ significantly decreases when γ is increased. Similarly, in order that appearance of the first muon predicted by this model be closer to the one predicted by the CYL approximation, the parameters $\beta = 0.5$ and $\gamma = 1.03$ are chosen for the IUFSU* case. Therefore, we can conclude that by observing the changes of Y_{Le}, Y_e, $Y_{L\mu}$, Y_μ with respect to the all parameters of $x_i(\rho_B)$ variations, the suitable parameters in Eq. (2) can be obtained. For the NL3 case, $x_{0e} = 0.08$, $x_{0m} = 1.0$, $\beta = 5$, and $\gamma = 2$, while for the IUFSU* case $x_{0e} = 0.2$, $x_{0m} = 0.3$, $\beta = 0.5$, and $\gamma = 1.03$. It also becomes obvious that the parameters β and γ control how fast and how smoothly Y_{L_e} reaches a constant value at high density. These parameters play a role also as a "fine tuner" to determine the correct density for the first muon appearance.

The fractions of each constituent which are predicted by the DDYL approach using the above $x_i(\rho_B)$ parameters for both parameter sets are compared to the corresponding ones predicted by the conventional CYL approach. The results are shown in Fig. 7. As expected, for each parameter set used, both approaches yield similar fraction predictions for every particle involved at high densities, including a quite correct density at which the first muon appears. However, at low densities, the DDYL approach yields significantly different behavior compared to that of CYL. In DDYL, the electron-neutrino population decreases when the baryon density approaches zero, while in CYL it slightly increases when the density approaches zero. Thus, for applications that need a transition from the inner crust with no trapped neutrinos to the low density of the core with trapped neutrinos, DDYL becomes more natural than CYL because a smooth transition between both regions can be more easily reached by the DDYL approach. In DDYL, the numbers of each charged particle (e and p) decrease faster compared to the ones of CYL when the baryon density approaches zero. DDYL predicts also increasing neutrons with a larger rate compared to the ones of CYL when the baryon density approaches zero. The immediate consequence of this "low density" difference appears in the stability of matter at low densities. We will discuss further in Sec. III. These similarities and differences in density profiles of electrons, muon populations, as well as proton and neutron populations can be understood from the trend of the electron, muon, and lepton chemical potentials predicted by both approaches that are shown in Fig. 8. One can observe, for each parameter set, the similarity in the density evolution trend of the muon chemical potential for all densities as well as of the electron and lepton chemical potentials at

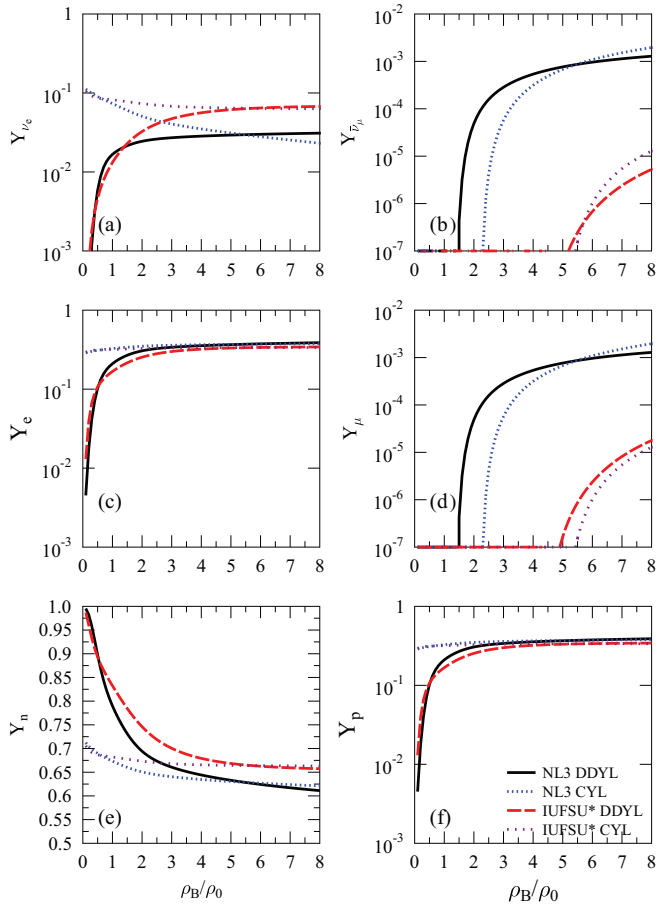

FIG. 7. (Color online) The effect of DDYL on PNS composition where the particles involved are ν_e, $\bar{\nu}_\mu$, e, μ, n, and p. IUFSU* and NL3 parameter sets are used. The fraction of (a) electron neutrinos, (b) muon antineutrinos, (c) electrons, (d) muons, (e) neutrons, and (f) protons. The corresponding results for the CYL approach are also given for the sake of comparison. The $T = 0$ approximation is used in the calculation.

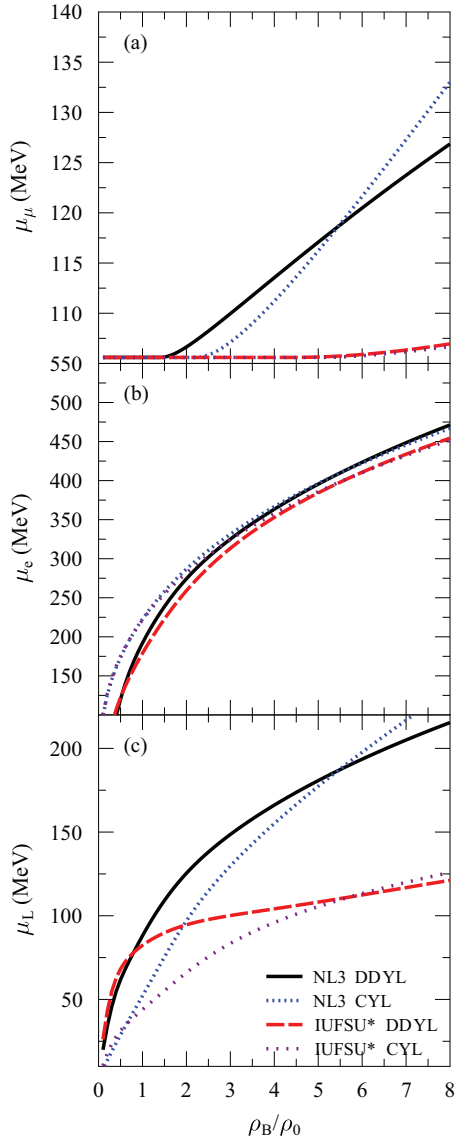

FIG. 8. (Color online) PNS lepton chemical potentials of (a) muons (μ_μ), (b) electrons (μ_e), and (c) leptons (μ_L). Other details as in Fig. 7.

high densities predicted by DDYL and CYL. The difference in the electron and lepton chemical potentials at low densities predicted by both approaches can be also clearly seen.

Note, from the studies of the luminosities and spectra of supernova neutrinos of different flavors [38] as well as the asymmetric neutrino emission driven by active-sterile neutrino oscillations in the PNS [39], it is evident that in the PNS the radius of the nonelectron neutrino sphere is shorter than the radius of the electron neutrino sphere. Therefore, the muons and taus cannot be present in the low-density region of PNS matter [6,17,40]. Thus, based on this fact, IUFSU* predicts a more reasonable fraction of muons than NL3 independently of the lepton fractions treatment used.

In the literature, there are many RMF parameter sets, which are introduced for different purposes. However, they can be classified roughly into two different stiffness characters of the EOS by looking at how fast the energy density of the corresponding EOS increased by increasing the pressure. It is known that the stiffest one is NL3 and the softest one is FSU, and the EOS stiffnesses of other parameter sets are in between the ones predicted by both parameter sets. Therefore, to see the effect of parameter set variation on particle populations predicted by the DDYL approach, beside NL3 and FSU, G1, G2, GM1, BSP, and IUFSU* are chosen to present the parameter sets with EOS stiffness less than that of NL3 but larger than that of FSU. We have found that roughly the x_{0e} of NL3, G1, G2, and GM1 are quite similar, i.e., $x_{0e} \sim 0.08$ while x_{0e} of IUFSU*, BSP, and FSU are $x_{0e} \sim 0.2$, so that we can use the $x_i(\rho_B)$ parameters of the NL3 and IUFSU* cases to calculate the particle populations using those parameter sets. The results are shown in Fig. 9. It is obvious that there is not any deviation observed of Y_{Le}, Y_e, $Y_{L\mu}$, Y_μ trends due to parameter set variation. Therefore, rough analysis above is valid also for these parameter sets. However, for G1, G2, GM1, BSP, and FSU parameter sets, a finer treatment of the location where the

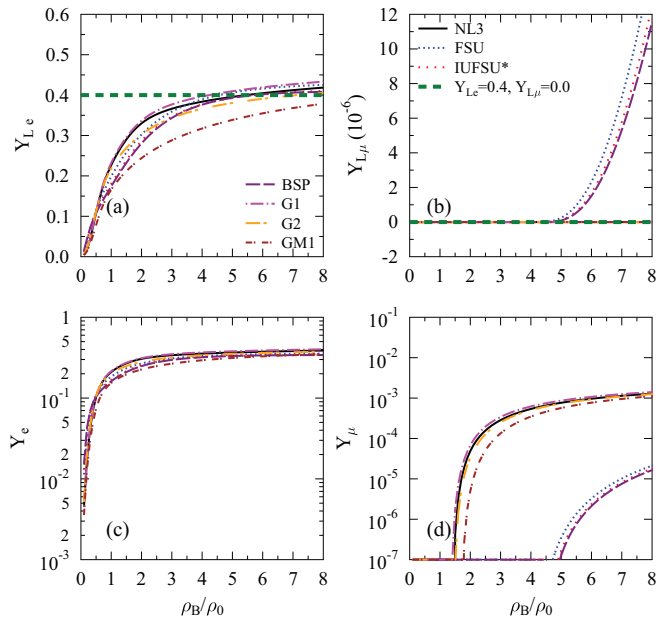

FIG. 9. (Color online) Lepton fractions predicted by some RMF parameter set representations using the DDYL approach.

muon appears for the first time, and a finer adjustments of γ and β parameters, are still needed.

Because the EOS of the PNS core is not too sensitive to the behavior at low densities, as expected, the difference due to the treatment of lepton fractions in the EOS cannot be observed. It happens not only in the case of soft EOS (IUFSU*) but also in the case stiff EOS (NL3). This is shown in Fig. 10. However, this result does not guarantee that both lepton fraction treatments (DDYL and CYL) produce identical PNS mass-radius relations or neutrino mean free paths in the PNS. These matters will be discussed in Secs. IV and V.

III. ONSET OF LOW-DENSITY INSTABILITY OF THE PNS

In this section we will discuss the effects of $x_i(\rho_B)$ parametrization in matter stability with respect to small density fluctuations, which in the thermodynamic method framework is usually called, loosely, mechanical stability [41].

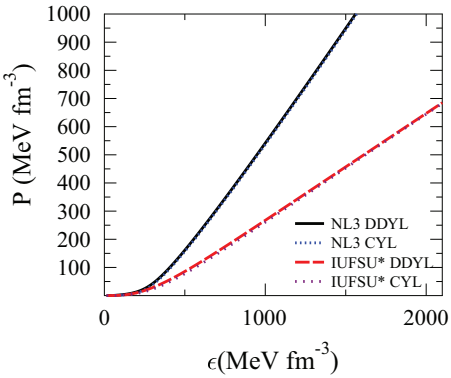

FIG. 10. (Color online) The effect of DDYL on the PNS EOS. Other details are as in Fig. 7.

Note that there are several methods to study the instability due to small density fluctuations in matter, such as the thermodynamic method [41–44], the relativistic [45,46] and nonrelativistic [47–49] dynamical methods, as well as the relativistic RPA based on the Green function formalism [50–52]. The thermodynamic method requires matter to fulfill not only the mechanical but also the chemical stability conditions [41,44]

$$-\left(\frac{\partial P}{\partial v}\right)_\mu > 0$$
$$-\left(\frac{\partial \mu}{\partial q_c}\right)_v > 0, \tag{11}$$

where v and q_c are the volume and charge per baryon number, while P and μ are the pressure and chemical potential. For dynamical models, the instability region of matter can be determined by examining when the convexity of the free-energy curvature is violated [45–49]. It was shown by Xu *et al.* [44] that thermodynamic stability is the limit of the nonrelativistic dynamical model as $k \to 0$ (long-wavelength limit) when the Coulomb interaction is neglected. On the other hand, it was known [45,46] that instabilities predicted by the relativistic dynamical method within the Landau-Vlasov formalism are indeed equivalent to those of teh relativistic RPA method. The relativistic RPA method requires longitudinal and transverse dielectric functions ε_L and $\varepsilon_T > 0$ when the time component of four-momentum $q_0 = 0$ to ensure the stability conditions, while in the low-density region the transverse instability part is absent. At high densities, the stabilities depend on the RMF nonlinear and isovector terms used (see more detail in Ref. [51]). Because the $x_i(\rho_B)$ parametrization is important only in the low-density region, here we focus only on small density fluctuation instability of the PNS matter in the low-density region.

The transition from the core to inner crust in the P(NS) matter takes place when the uniform ground state of matter which is used to describe the core becomes unstable to small density fluctuations with the momentum transfer q. This happens when [52]

$$\varepsilon_L = \det[1 - D_L(q)\Pi_L(q, q_0 = 0)] \leqslant 0. \tag{12}$$

In Eq. (12) q_0 is the time component of the four-momentum transfer $q^\mu = (q_0, \vec{q}\,)$ and $q = |\vec{q}\,|$. The onset of instability can be extracted from this condition, and the transition density from core to inner crust ρ_t can be approximated as the largest density for which the above condition has a solution. The explicit form of each element in the longitudinal meson propagator and longitudinal polarization matrices $D_L(q)$ and Π_L can be seen in Refs. [30,31,52].

As briefly mentioned in the Introduction, matter with neutrino trapping within the CYL approach predicts a relatively larger ρ_t than that predicted by matter without neutrino trapping. However, the ρ_t difference predicted by both types of matter is rather model dependent. For example, RMF models which use nonlinear terms including mixing between vector isoscalars and vector isovectors predict relatively smaller ρ_t difference compared to that of the RMF models which do not use this mixing term. Furthermore, the difference becomes

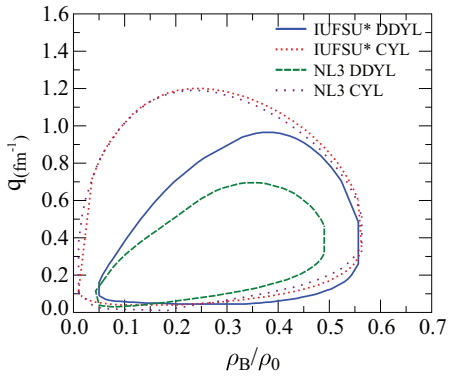

FIG. 11. (Color online) The effect of DDYL on the onset of PNS longitudinal instability at low densities as a function of the ratio between baryon and nuclear saturation densities and perturbation momentum. Other details are as in Fig. 7.

insignificant if a relatively large coupling of this mixing term is used [30]. In general, the onset of instability of matter with neutrino trapping is significantly larger than that of matter without neutrino trapping. In contrast to the unstable region predicted by matter without neutrino trapping, the unstable region predicted by matter with neutrino trapping is only modestly influenced by symmetry energy behavior at high density. From the point of view of interactions among the constituents involved at low density, these results can be understood [31,32]. The consequence of suppressing electron and proton populations at low densities by using the DDYL approach is that the onset of instability in PNS matter becomes significantly reduced while the narrowness of the unstable region depends on the parameter set used. NL3 yields a narrower unstable region compared to the one predicted by IUFSU*. As expected, CYL yields a broader unstable region and is almost independent of the parameter set used. These results are shown in Fig. 11. Note that the unstable region also depends on temperature. For the CYL case, it is known that the ρ_t decreases by increasing temperature and the unstable region becomes narrower when the temperature increases [53].

The ρ_t and P_t results can be seen in Table I. For both parameter sets, CYL yields larger ρ_t compared to the one predicted by DDYL, but the effect appears more significantly for NL3 case than that for IUFSU* case. The P_t result is rather model dependent. A parameter set with stiff EOS yields larger P_t than that of a soft EOS. If the PNS ρ_t predicted by both approaches are compared to the ρ_t of NS, then for each parameter set, it is obvious that the ρ_t predicted by DDYL is closer to the corresponding ρ_t of NS compared to that of CYL. The difference in ρ_t and P_t predictions of CYL and DDYL will yield observed effect for PNS radius. This matter will be discussed in the next section.

IV. MASS-RADIUS RELATION OF THE PNS

In this section, the effect of the DDYL approach on mass and radius of the PNS is qualitatively investigated. The static $T = 0$ PNS mass-radius relation is calculated by solving the Tolman-Oppenheimer-Volkov (TOV) equation. The outer crust region of the PNS is roughly assumed to have the same form as the one used for a NS, i.e., by using the outer crust EOS of Rüster *et al.* [54]. This EOS is a recent version of the one introduced by Baym, Pethick, and Sutherland [55]. Because the detailed EOS of the neutrino sphere (inner crust) is not certain, the relation of polytrophic pressure to energy density usually used for a NS calculation is used here also to interpolate the EOS for regions between the outer crust and the core [28]. The core of the PNS is calculated by using the IUFSU* and NL3 parameter sets, and for lepton fractions treatment the CYL and DDYL approaches are employed. The polytrophic parameters A and B of the inner crust are determined from the pressures and energy at ρ_t of the core and $\rho_{\rm max}$ of the outer crust, where their explicit values can be seen in Table I. Note that the PNS properties based on the RMF model using the CYL approach for an isentropic process with $s = 1$ and 2 have been discussed in many places, e.g., Refs. [6,56]. The temperature correction in the PNS maximum mass to the one obtained by zero-temperature approximation is around $\alpha s^2 M_{\rm max}(0)$ [6], where the parameter α depends on the EOS used and, in general, α is around 10^{-2}. Thus it seems that the temperature correction for the $s = 1$ case plays less of a role for increasing PNS maximum mass. The effect of DDYL with varied constituents involved and the isentropic process has been also discussed in Ref. [19]. The importance of the presence of hyperons is also included in that paper. However, they used a different way of $x_i(\rho_B)$ parametrization than the one used in this work.

The PNS mass-radius plots which are calculated by using NL3 and IUFSU* parameter sets as well as by implementing DDYL and CYL approaches to treat the lepton fractions are shown in Fig. 12. For the sake of comparison, NS mass-radius results are also shown. It is obvious that NL3 yields larger

TABLE I. Tabulation of some PNS crust properties such as density and pressure at the core-crust transition region and polytrophic EOS parameters A and B at the inner crust. All properties are calculated by using the $T = 0$ approximation. For the sake of comparison, the values of these properties for NS matter are also provided.

Force	P_t (MeV fm^{-3})	ρ_t (fm^{-3})	A (MeV fm^{-3})	B (MeV$^{1/3}$fm^{-1})
IUFSU* DDYL	0.7005	0.0846	1.725×10^{-4}	2.019×10^{-3}
IUFSU* CYL	0.8170	0.0856	1.353×10^{-4}	2.248×10^{-3}
IUFSU* NSM	0.3015	0.0810	3.505×10^{-4}	0.919×10^{-3}
NL3 DDYL	1.0917	0.0734	-1.182×10^{-4}	3.814×10^{-3}
NL3 CYL	1.0375	0.0840	0.243×10^{-4}	2.934×10^{-3}
NL3 NSM	0.2135	0.0540	3.063×10^{-4}	1.192×10^{-3}

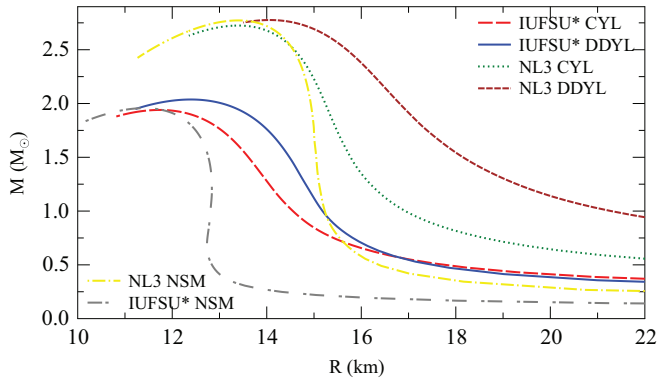

FIG. 12. (Color online) PNS mass-radius relation for various matter compositions. NS results (NSM) are also shown for the sake of comparison. Other details are as in Fig. 7.

maximum masses for all cases than those of IUFSU* because the EOS of NL3 are significantly stiffer than that of IUFSU*. For each parameter set, the radius of the PNS is larger than the one of the NS because the transition density and its corresponding pressure of the PNS are larger than the ones of the NS, so the PNS has a wider transition region (inner crust) between core and the outer crust (see Table I for explicit values). However, the important thing here is the significant effects observed if we compare the DDYL with the CYL results. For each parameter set, DDYL yields slightly larger maximum mass and larger radius for canonical mass ($1.4M_\odot$). For the case of radius, the effect is more dramatic when the EOS is stiffer. Note that many works have been devoted recently to constrain the mass and radius of an NS from nuclear physics and astrophysics points of view [57–62]. However, unlike the NS case, there is no existing phenomenological constraint that can be compared to the PNS mass or radius calculation results.

In the case of PNS minimum mass, to obtain an accurate result one should treat consistently the finite-temperature effect of the EOS as well as an appropriate EOS for the outer crust to obtain the correct property prediction of the minimum mass of the PNS. However, because we want only to estimate qualitatively the effect of DDYL in the core region close to the crust, the following discussion seems in order. Recent studies in this direction by using Brueckner theory can be found e.g., in Ref. [17]. They found the minimum mass $0.58 \leqslant M_{\rm min} \leqslant 0.60\, M_\odot$ with $38 \leqslant R_{\rm min} \leqslant 44$ km for the case $s = 1$. Moreover, $0.70 \leqslant M_{\rm min} \leqslant 0.77\, M_\odot$ with $42 \leqslant R_{\rm min} \leqslant 52$ km for the case $s = 2$. The center density for $s = 1$ is around $\rho_c \approx \rho_0$ and for $s = 2$ around $\rho_c \approx 0.9\rho_0$. In both cases, the results depend significantly on the low-density EOS used. In Table II, the NS masses, radii, as well as Y_{ν_e}'s of NL3 and IUFSU* parameter sets using DDYL and CYL approaches at fixed center density $\rho_c \approx \rho_0$ are shown. The masses and radii are relatively smaller than the results of Ref. [17]. The important thing is that, for each parameter set, the DDYL approach yields larger minimum mass but shorter radius compared to the ones predicted by CYL. For the mass case, the effect is more pronounced for a parameter set with stiff EOS, but for the radius case the effect is more significant for soft EOS. It can be observed that PNS matter with DDYL predicts

TABLE II. Tabulation of some PNS properties at $\rho_c/\rho_0 \approx 1$ such as neutrino fraction at the center, masses as a function of solar mass ($M_\odot$), and radii in km for DDYL and CYL approaches. All properties are calculated by using the $T = 0$ approximation.

Force	P_c (MeV fm^{-3})	Y_{ν_e}	$M/M_\odot$	R (km)
IUFSU* DDYL	3.76	1.3×10^{-2}	0.34	21.67
IUFSU* CYL	3.21	8.2×10^{-2}	0.32	26.74
NL3 DDYL	5.73	1.7×10^{-2}	0.74	26.18
NL3 CYL	4.13	7.3×10^{-2}	0.46	26.73

more less one order of magnitude smaller Y_{ν_e} at the center of the PNS compared to that of CYL, while it is known that the center density is sensitive to Y_{ν_e}. Thus, the difference in mass and radius predictions between CYL and DDYL are mainly due to the Y_{ν_e} difference at center between the one of CYL and the one of DDYL. We believe that this behavior might be retained if we properly take into account finite temperature effects.

In addition, we need to note that many works have been devoted to study the convective instability in the PNS using different methods [63–66]. A negative gradient in the lepton number has been known to lead to convection during the cooling phase of the PNS [63,64]. However, the recent study by the authors of Ref. [13] using the requirement that the linear growth rates which are obtained from Ledoux analysis $\omega^2 > 0$, has found that the negative entropy gradients always yield a destabilizing effect. The sign and magnitude of the $(\frac{\partial \ln P}{\partial \ln Y_L})_{\rho_B,S}$ in the second term of the growth depend strongly on the nuclear symmetry energy. Therefore, negative gradients in lepton number can either stabilize or destabilize matter with respect to the convection, and the degree of stabilization depends on the RMF parameter set used. Off course, this field of study is important, but it is already outside the scope of this present work. However, here, we only want to argue that the $x_i(\rho_B)$ parametrization might also influence the gradient of the lepton number for the PNS because, unlike the one of CYL, the Y_L of DDYL is decreasing when it reaches the edge of the star, and if it is included in a realistic calculation it might provide the observed effect. We plot the lepton fraction as a function radius and mass developments of a PNS with $M = 1.9M_\odot$, where its center density is varied depending on the parameter set used, in the lower and upper panels of Fig. 13 to show this effect.

V. ELECTRON NEUTRINO MEAN FREE PATH IN THE PNS

In this section we will discuss how the neutrino mean free path is affected by $x_i(\rho_B)$ parametrization. A brief formulation of the neutrino mean free path is given then the result is discussed.

For electron-neutrino matter interactions based on the standard model of weak interaction, the differential scattering cross section has the form

$$\frac{1}{V}\frac{d^3\sigma}{d^2\Omega' dE'_\nu} = -\frac{G_F}{32\pi^2}\frac{E'_\nu}{E_\nu}\mathrm{Im}(L_{\mu\nu}\Pi^{\mu\nu}). \qquad (13)$$

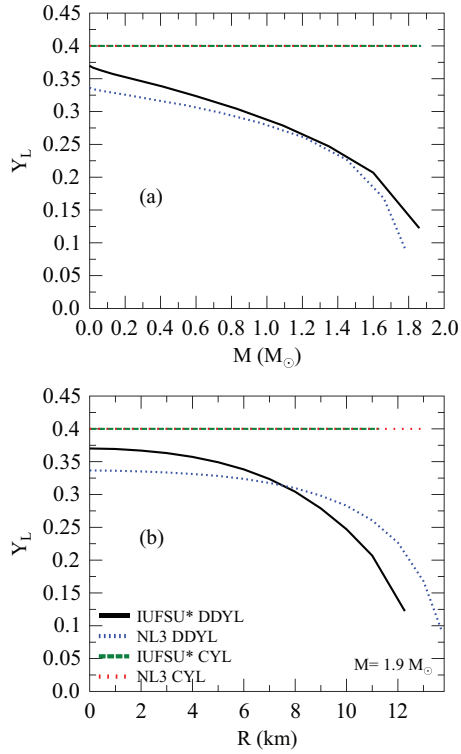

FIG. 13. (Color online) PNS lepton fractions as a function of PNS (a) mass and (b) radius. Other details as in Fig. 7.

Here E_ν and E'_ν are the initial and final neutrino-electron energies, respectively. $G_F = 1.023 \times 10^{-5}/M^2$ is the weak coupling, and M is the nucleon mass. The explicit forms of electron-neutrino tensor $L_{\mu\nu}$ and polarization tensor $\Pi^{\mu\nu}$ in the mean field approximation can be seen for example in Ref. [67]. The matter effects enter into calculation through $\Pi^{\mu\nu}$ because each component of $\Pi^{\mu\nu}$ depends on the effective mass and effective energy of each constituent of matter. The electron-neutrino mean free path (λ) in the $T = 0$ approximation as a function of initial neutrino energy at a certain density is obtained by integrating the cross section into the time and vector components of the neutrino momentum transfer, i.e,

$$\frac{1}{\lambda(E_\nu)} = \int_{q_0}^{2E_\nu - q_0} d|\vec{q}| \int_0^{2E_\nu} dq_0 \frac{|\vec{q}|}{E'_\nu E_\nu} 2\pi \frac{1}{V} \frac{d^3\sigma}{d^2\Omega' dE'_\nu}. \tag{14}$$

The electron neutrino mean free path (λ) results for NL3 and IUFSU* parameter sets by using DDYL and CYL approaches in treating the lepton fractions as a function of baryon density as well as the PNS radius for a PNS with $M = 1.9M_\odot$ are shown in Fig. 14. Here $E_{\nu_e} = 5$ MeV and $E_{\nu_e} = 10$ MeV are taken and the $T = 0$ approximation is used. It can be observed from panel (c) of Fig. 14 that the difference in λ predicted by NL3 and IUFSU* appears in region $\rho_0 \leqslant \rho_B \leqslant 4\rho_0$. NL3 yields rather irregular behavior of λ, i.e., λ increases up to a certain density and then decreases again with respect to increasing baryon density, while the one of IUFSU* do not show such behavior. This means that the λ in PNS matter is quite model dependent. However, our interest here is mainly at $\rho_B \leqslant \rho_0$, where for each parameter set DDYL yields relatively

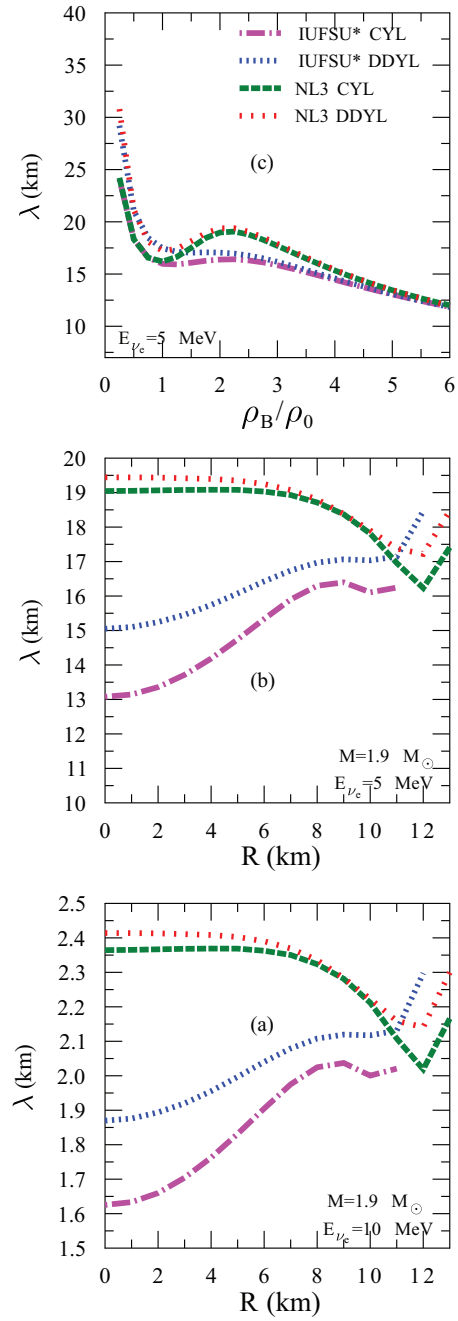

FIG. 14. (Color online) The mean free path (λ) of electron neutrinos using DDYL and CYL approaches which are predicted by IUFSU* and NL3 parameter sets. (a) λ as a function of PNS radius in the case $E_{\nu_e} = 10$ MeV and $M = 1.9M_\odot$. (b) λ as a function of PNS radius in the case $E_{\nu_e} = 5$ MeV and $M = 1.9M_\odot$. (c) λ as a function of the ratio between baryon and nuclear saturation densities with $E_{\nu_e} = 5$ MeV. Other details are as in Fig. 7.

larger λ compared to that of CYL. From the plot in panel (c) of Fig. 14, it can be observed that the effect does not seem too significant, but if we look at λ as a function of star radius with fixed mass, e.g., $M = 1.9M_\odot$, as shown in panels (a) and (b), then the effect can be seen more clearly. However, the effect depends strongly on the parameter set used. For NL3 the effect is small but for IUFSU* it becomes quite significant.

The neutrino energy affects only the magnitude but not the trend of λ with respect to the baryon density evolution. However, if the mass of the star is changed, the trend of λ with respect to the baryon density evolution is slightly changed, but still the DDYL yields larger λ compared to that of CYL. Therefore, in general, the effect of DDYL on the PNS EOS compared to CYL is that the matter is more transparent with respect to electron-neutrino transport, where the degree of the transparency of the matter depends on parameter set used. This fact might influence neutrino emission from a newly born NS or PNS cooling.

VI. CONCLUSION

We have studied systematically the DDYL approach which is proposed by Ryu *et al.* [19] in the $T = 0$ approximation. Two sets of the neutrino-to-electron ratio parameters of this approach are found. One can be used for the RMF parameter set with stiff EOS and the other for soft EOS. They yield profiles of particle composition at high densities similar to the corresponding results predicted by the conventional CYL approach. However, at low densities, the DDYL approach yields significantly different profile behavior than that of CYL. The DDYL produces a decreasing neutrino-electron number when the baryon density goes to zero. Therefore, it seems quite natural to describe a smooth transition from the inner crust without neutrino trapping to the core with neutrino trapping by using the DDYL approach. To obtain the parameters of the neutrino-to-lepton ratio in Eq. (2), the constraints $Y_{Le} \sim 0.4$ at high densities, $Y_{Le} \sim 0$ for all densities, as well as a parameter fine-tuning in order that the first muon appears at a quite appropriate density, are used. To see impacts of DDYL on some PNS properties where the information might be useful for core-collapse modeling, the EOS, low-density instability of matter, mass-radius relation of the star, and electron neutrino mean free path in this matter are calculated. The results are compared to the ones obtained by using the conventional CYL approach. The DDYL yields smaller onset of low instability and core-crust transition density ρ_t than the ones of CYL because DDYL predicts fewer leptons at low densities. The ρ_t which is predicted by DDYL is closer to that obtained for a NS than that of CYL. These effects are, however, rather sensitive to the RMF parameter set used. Therefore, even DDYL only modestly influences the EOS, the radius of canonical PNS mass yielded by using the DDYL approach is larger than that of CYL due to the ρ_t difference predicted by the two approaches. The explicit manifestation of this difference is in the size difference of the PNS inner crust. Concerning the PNS minimum mass, even this is rather parameter-set dependent, but in general the DDYL approach yields larger minimum mass but shorter radius compared to those predicted by CYL. This effect is due to, in the PNS center, DDYL yielding a Y_{ν_e} which is more less one order of magnitude larger than the one predicted by CYL. A possibility that DDYL also influences the PNS convective instability is also discussed. For electron-neutrino transport in the PNS, even though the result is also rather parameter-set dependent, it is found that the matter obtained by using DDYL is more transparent than that obtained by using CYL. We want to point out that, in the present work, the finite temperature correction is not included, which is important for more quantitative results. However, we believe that the effects that we have already discussed in this work are still retained for a realistic calculation.

ACKNOWLEDGMENT

A.S. acknowledges the support given by Universitas Indonesia through Hibah RUUI 2012.

[1] H. A. Bethe, Rev. Mod. Phys. **62**, 801 (1990).
[2] S. E. Woosley and T. A. Weaver, Astrophys. J. Suppl. **101**, 181 (1995).
[3] S. U. Scheidegger, Ph.D. Thesis, University of Basel, 2010 (unpublished).
[4] A. Burrows and J. M. Lattimer, Astrophys. J. **307**, 178 (1986).
[5] H. Chen, M. Baldo, G. F. Burgio, and H.-J. Schulze, Phys. Rev. D **84**, 105023 (2011).
[6] M. Prakash, I. Bombaci, M. Prakash, P. J. Ellis, J. M. Lattimer, and R. Knorren, Phys. Rep. **280**, 1 (1997).
[7] M. Oertel, A. F. Fantina, and J. Novak, Phys. Rev. C **85**, 055806 (2012).
[8] J. M. Lattimer and F. D. Swesty, Nucl. Phys. A **535**, 331 (1991).
[9] H. Shen, H. Toki, K. Oyamatsu, and K. Sumiyoshi, Nucl. Phys. A **637**, 435 (1998).
[10] M. Hampel and J. Schaffner-Bielich, Nucl. Phys. A **837**, 210 (2010).
[11] I. Sagert, M. Hempel, G. Pagliara, J. Schaffner-Bielich, T. Fischer, A. Mezzacappa, F.-K. Thielemann, and M. Liebendörfer, Phys. Rev. Lett. **102**, 081101 (2009).
[12] K. Sumiyoshi, C. Ishizuka, A. Ohnishi, and H. Suzuki, Astrophys. J. Lett. **690**, L43 (2009).
[13] L. F. Roberts, G. Shen, V. Cirigliano, J. A. Pons, S. Reddy, and S. E. Woosley, Phys. Rev. Lett. **108**, 061103 (2012).
[14] J. M. Lattimer and Y. Lim, arXiv:1203.4286.
[15] D. Gondek, P. Haensel, and J. L. Zdunik, Astron. Astrophys. **325**, 217 (1997).
[16] K. Strobel and M. K. Weigel, Astron. Astrophys. **367**, 582 (2001).
[17] G.-F. Burgio and H.-J. Schulze, Astron. Astrophys. **518**, A17 (2010).
[18] K. Strobel, Ch. Schaab, and M. K. Weigel, Astron. Astrophys. **350**, 497 (1999).
[19] C. Y. Ryu, T. Maruyama, T. Kajino, and M.-K. Cheoun, Phys. Rev. C **83**, 018802 (2011).
[20] T. Fischer, S. C. Whitehouse, A. Mezzacappa, F.-K. Thielemann, and M. Liebendörfer, Astron. Astrophys. **499**, 1 (2009).
[21] J. A. Pons, S. Reddy, M. Prakash, J. M. Lattimer, and J. A. Miralles, Astrophys. J. **513**, 780 (1999).
[22] S. Reddy, M. Prakash, and J. M. Lattimer, Phys. Rev. D **58**, 013009 (1998).
[23] C. Y. Ryu, T. Maruyama, T. Kajino, G. J. Mathews, and M.-K. Cheoun, Phys. Rev. C **85**, 045803 (2012).
[24] G. A. Lalazissis, J. Konig, and P. Ring, Phys. Rev. C **55**, 540 (1997).

[25] B. K. Agrawal, A. Sulaksono, and P.-G. Reinhard, Nucl. Phys. A **882**, 1 (2012).
[26] R. Furnstahl, B. D. Serot, and H.-B. Tang, Nucl. Phys. A **615**, 441 (1997).
[27] N. K. Glendenning and S. A. Moszkowski, Phys. Rev. Lett. **67**, 2414 (1991).
[28] F. J. Fattoyev, C. J. Horowitz, J. Piekarewicz, and G. Shen, Phys. Rev. C **82**, 055803 (2010).
[29] C. Ducoin, J. Margueron, C. Providencia, and I. Vidaña, Phys. Rev. C **83**, 045810 (2011).
[30] A. Sulaksono and T. Mart, Phys. Rev. C **74**, 045806 (2006).
[31] T. Mart and A. Sulaksono, Phys. Rev. C **78**, 025808 (2008).
[32] T. Mart and A. Sulaksono, Mod. Phys. Lett. A **24**, 1059 (2009).
[33] C. J. Horowitz and M. A. Perez-Garcia, Phys. Rev. C **68**, 025803 (2003).
[34] L. Mornas and A. Perez, Eur. Phys. J. A **13**, 383 (2002).
[35] A. Burrows and R. F. Sawyer, Phys. Rev. C **58**, 554 (1998); **59**, 510 (1999).
[36] S. Reddy, M. Prakash, J. M. Lattimer, and J. A. Pons, Phys. Rev. C **59**, 2888 (1999).
[37] A. Sulaksono, C. K. Williams, P. T. P. Hutauruk, and T. Mart, Phys. Rev. C **73**, 025803 (2006).
[38] H.-T. Janka, Astropart. Phys. **3**, 377 (1995).
[39] M. Barkovich, J. C. D'Olivio, and R. Montemayor, in *Trends in Pulsar Research* (Nova Science, New York, 2007), p. 119.
[40] A. Rabhi, P. K. Panda, and C. Providência, Phys. Rev. C **84**, 035803 (2011).
[41] S. Kubis, Phys. Rev. C **76**, 025801 (2007); **70**, 065804 (2004).
[42] M. Lattimer and M. Prakash, Phys. Rep. **333**, 121 (2000); Astrophys. J. **550**, 426 (2001).
[43] B-A. Li, A. T. Sustich, M. Tilley, and B. Zhang, Nucl. Phys. A **699**, 493 (2002).
[44] J. Xu, L.-W. Chen, B.-A. Li, and H.-R. Ma, Astrophys. J. **697**, 1549 (2009).
[45] M. Nielsen, C. Providência, and J. da Providência, Phys. Rev. C **44**, 209 (1991).
[46] C. Providência, L. Brito, S. S. Avancini, D. P. Menezes, and Ph. Chomaz, Phys. Rev. C **73**, 025805 (2006).
[47] C. J. Pethick, D. G. Ravenhall, and C. P. Lorenz, Nucl. Phys. A **584**, 675 (1995).
[48] F. Douchin and P. Haensel, Phys. Lett. B **485**, 107 (2000).
[49] C. Ducoin, Ph. Chomaz, and F. Gulminelli, Nucl. Phys. A **789**, 403 (2007).
[50] K. Lim and C. J. Horowitz, Nucl. Phys. A **501**, 729 (1989).
[51] A. Sulaksono, T. J. Bürvenich, P.-G. Reinhard, and J. A. Maruhn, Phys. Rev. C **79**, 044306 (2009); A. Sulaksono, T. Mart, T. J. Bürvenich, and J. A. Maruhn, *ibid.* **76**, 041301(R) (2007).
[52] J. Carriere, C. J. Horowitz, and J. Piekarewicz, Astrophys. J. **593**, 463 (2003).
[53] J. Xu, L.-W. Chen, C. M. Ko, and B.-A. Li, Phys. Rev. C **81**, 055805 (2010).
[54] S. B. Ruster, M. Hempel, and J. Schaffner-Bielich, Phys. Rev. C **73**, 035804 (2006).
[55] G. Baym, C. Pethick, and P. Sutherland, Astrophys. J. **170**, 299 (1971).
[56] I. Bednarek and R. Manka, Phys. Rev. C **73**, 045804 (2006).
[57] K. Hebeler, J. M. Lattimer, C. J. Pethick, and A. Schwenk, Phys. Rev. Lett. **105**, 161102 (2010).
[58] P. B. Demorest, T. Pennucci, S. M. Ransom, M. S. E. Roberts, and J. W. T. Hessels, Nature (London) **467**, 1081 (2006).
[59] F. Özel, G. Baym, and T. Guver, Phys. Rev. D **82**, 101301 (2010).
[60] A. W. Steiner, J. M. Lattimer, and E. F. Brown, Astrophys. J. **722**, 33 (2010).
[61] V. Suleimanov, J. Poutanen, M. Revnivtsev, and K. Werner, Astrophys. J. **742**, 122 (2011).
[62] A. W. Steiner, J. M. Lattimer, and E. F. Brown, Astrophys. J. **765**, L5 (2013).
[63] R. I. Epstein, Mon. Not. R. Astron. Soc. **188**, 305 (1979).
[64] J. J. Zach, Phys. Rev. D **65**, 123002 (2002).
[65] W. Keil, H.-T. Janka, and E. Müller, Astrophys. J. **473**, L111 (1996).
[66] J. A. Miralles, J. A. Pons, and V. A. Urpin, Astrophys. J. **574**, 356 (2002).
[67] A. Sulaksono, P. T. P. Hutauruk, and T. Mart, Phys. Rev. C **72**, 065801 (2005).